

Elastic constants and the formation of topological defects in hybrid nematic cells: A Monte Carlo study

Cesare Chiccoli,¹ Paolo Pasini,¹ Luiz Roberto Evangelista,² Gregor Skačej,³
Rodolfo Teixeira de Souza,⁴ and Claudio Zannoni⁵

¹*INFN, Sezione di Bologna, Via Irnerio 46, I-40126 Bologna, Italy*

²*Departamento de Física, Universidade Estadual de Maringá, Avenida Colombo, 5790-87020-900 Maringá (PR), Brazil*

³*Faculty of Mathematics and Physics, University of Ljubljana, Jadranska 19, SI-1000 Ljubljana, Slovenia*

⁴*Departamento Acadêmico de Física, Universidade Tecnológica Federal do Paraná, Campus Apucarana,
Rua Marçílio Dias, 635 CEP 86812-460 – Apucarana (PR), Brazil*

⁵*Dipartimento di Chimica Industriale “Toso Montanari” and INSTM, Università di Bologna, Viale Risorgimento 4, I-40136 Bologna, Italy*



(Received 14 July 2020; accepted 2 October 2020; published 20 October 2020)

We present a Monte Carlo study of the effects of elastic anisotropy on the topological defects which can be formed in nematic films with hybrid boundary conditions. We simulate the polarized microscopy images and analyze their evolution in uniaxial systems for different values of the Frank elastic constants.

DOI: [10.1103/PhysRevE.102.042702](https://doi.org/10.1103/PhysRevE.102.042702)

I. INTRODUCTION

Liquid crystals (LCs) are materials that present one or more state of aggregation, with some degree of order and fluidity, intermediate between isotropic liquids and solid crystals [1,2]. The main realm of liquid-crystal phases is in condensed matter physics and technology, but systems with surprising analogies have now emerged in fields of physics as diverse as nuclear research [3,4] and cosmology [5,6]. One of the most interesting aspects of LC materials is the formation of various types of topological defects [7] due to the deformations induced by some external fields or boundary conditions that contrast the tendency of the constituent particles (e.g., molecules or spins) to align along a preferred direction called a director. Then points, lines, and walls where the director cannot be defined can be formed at the boundary of domains or regions with different alignments. It is also well known that for some real materials, for example, 5CB [8], disclination lines can be formed in a perfect hybrid aligned nematic (HAN) where the alignment at one of the two flat surfaces confining the nematic is homeotropic, i.e., perpendicular to the surface (say, at $z = h$) and at the other (at $z = 0$) is parallel to the surface, either randomly distributed [9] or aligned along the x or y axes [10]. HAN cells are interesting for technological applications [11] since their molecular organization and their birefringence can be changed by an external field applied across the cell in a continuous way, without the threshold involved, e.g., in planar aligned cells for a nematic with positive diamagnetic anisotropy and a perpendicular magnetic field applied (Fréedericksz transition [1,12]). It should also be mentioned that the confining surfaces are not necessarily solid, e.g. thin films of 5CB drops deposited on a glycerol surface, which induces tangential alignment, while having a homeotropic alignment at the free air interface, have been studied [13]. HAN features are similar to those that can be obtained for a nematic confined

between two horizontally aligning surfaces and subject to the action of a vertical external field as, for example, studied many years ago by Leger [14]. We have confirmed these results by computer simulations of a hybrid cell with homeotropic and fully degenerate [15], partially ordered [9], or uniform with a small pretilt [16] planar boundary conditions using a pseudopair potential, introduced by Gruhn and Hess [17] and by Romano and Luckhurst [18–21] (GHRL), which takes into account the main Frank elastic constants, the splay (K_1), twist (K_2), and bend (K_3) ones. The disclination lines were obtained not only using the GHRL model with the elastic constants of 5CB but also in the one-constant approximation, i.e., $K_1 = K_2 = K_3$. In this limit the GHRL potential reduces to the Lebwohl-Lasher (LL) Hamiltonian [22,23], which in turn was the first successful lattice model introduced to simulate the orientational properties of nematics. Even if the one elastic constant approximation is most often used in theoretical work because of its simplicity [12], it is important to study nematic films allowing for elastic constant anisotropy. Indeed, even if for low molar mass liquid crystals the differences between the K_i constants are normally relatively small, the need to account in a simple way for differences in elastic constants is essential for a variety of systems such as LC polymers [24,25], LCs originating from a long virus such as the tobacco mosaic virus (TMV) [26], nanotubes [27] or other nanocrystal suspensions [28], and for low molar mass nematics approaching a smectic phase, where the bend elastic constant is expected to diverge [1]. Relating elastic constants to polarized optical microscopy (POM) textures is important also in view of the possibility of determining the elastic constant anisotropy *in situ* from polarized optical microscopy textures and not from separate experiments in the bulk, e.g., from the already mentioned Fréedericksz director configuration transition, upon applying a sufficiently strong external field [1,12]. Various numerical treatments based on continuum theory have been put forward,

particularly by Windle and co-workers [29], Sonnet, Kilian, and Hess [30], and Kilian and Hess [31]. Measuring geometrical features such as disclination radii of the $s = 1/2$ defects has also been suggested as a means to determine at least some elastic constants in polymer liquid-crystal disclinations directly from transmission electron microscopy (TEM) images [32,33]. The general problem of molecular organization in a HAN cell is, however, complicated as different factors in addition to elastic constants can come into play, such as the roughness and the geometric details of the confining surface [34] and the effect of surface anchoring strength that we have examined in a previous work [16].

Here, we aim to employ Monte Carlo (MC) simulations to provide a convenient link between the elastic constants of the nematic in a HAN cell with homeotropic and uniform planar boundaries and their polarized optical images as obtained in real experiments. As in a previous study on spherical droplets [35], we try to build a small catalog that can hopefully be of help to experimentalists.

II. THE MODEL SYSTEMS

The GHRL potential [17,20] consists of a system of interacting centers (“spins”) placed at the sites of a certain regular lattice. The Hamiltonian is written as follows,

$$U_N = \frac{1}{2} \sum_{i,j \in F} \sum_{i \neq j} \Phi_{ij} + J \sum_{i \in F} \sum_{j \in S} \Phi_{ij}, \quad (1)$$

where F, S are the set of particles in the bulk and at the surfaces, respectively, and the parameter J models the strength of the coupling with the surfaces (assumed to be the same). The particles interact through the second rank attractive pair potential,

$$\begin{aligned} \Phi_{ij} = & \epsilon \{ \lambda [P_2(\mathbf{u}_i \cdot \mathbf{s}) + P_2(\mathbf{u}_j \cdot \mathbf{s})] \\ & + \mu [(\mathbf{u}_i \cdot \mathbf{s})(\mathbf{u}_j \cdot \mathbf{s})(\mathbf{u}_i \cdot \mathbf{u}_j) - 1/9] \\ & + \nu P_2(\mathbf{u}_i \cdot \mathbf{u}_j) + \rho [P_2(\mathbf{u}_i \cdot \mathbf{s}) \\ & + P_2(\mathbf{u}_j \cdot \mathbf{s})] P_2(\mathbf{u}_i \cdot \mathbf{u}_j) \}, \end{aligned} \quad (2)$$

where i, j are nearest neighbors ($\Phi_{ij} = 0$ otherwise) and

$$\lambda = \frac{1}{3} \Lambda (2K_1 - 3K_2 + K_3), \quad (3a)$$

$$\mu = 3\Lambda (K_2 - K_1), \quad (3b)$$

$$\nu = \frac{1}{3} \Lambda (K_1 - 3K_2 - K_3), \quad (3c)$$

$$\rho = \frac{1}{3} \Lambda (K_1 - K_3), \quad (3d)$$

with K_1, K_2, K_3 being the splay, twist, and bend Frank elastic constants [1,12], Λ a factor with the dimensions of length related to the dimension of the unit cell [21], and $\mathbf{s} = \mathbf{r}/|\mathbf{r}|$, $\mathbf{r} = \mathbf{x}_i - \mathbf{x}_j$, with $\mathbf{x}_i, \mathbf{x}_j$ the dimensionless coordinates of the i th and j th lattice points. $\mathbf{u}_i, \mathbf{u}_j$ are unit vectors along the axis of the two particles (“spins”) and P_2 is a second rank Legendre polynomial. The relation between the three elastic constants and the four potential coefficients is completed by setting the condition $\mu = -3(\rho + \lambda)$, which is needed to ensure that two parallel neighbor spins always have the same

TABLE I. As an example of the correspondence of the elastic constants, $K_i^* = K_i \times 10^{12}$ N, with the values of the parameters, λ, μ, ρ , and ν , appearing in the potential, we report the limiting cases studied in the present simulations. The values of λ, μ , and ρ are normalized to have $\nu = -1$.

K_1^*	K_2^*	K_3^*	λ	μ	ν	ρ
1	1	1	0.0000	0.0000	-1.0000	0.0000
1	1	9	0.7273	0.0000	-1.0000	-0.7273
1	9	1	-0.8889	2.6667	-1.0000	0.0000
1	9	9	-0.4571	2.0571	-1.0000	-0.2286
9	1	1	-3.2000	14.4000	-1.0000	-1.6000
9	1	9	8.0000	-24.0000	-1.0000	0.0000
9	9	1	-0.4211	0.0000	-1.0000	0.4211

interaction energy, independent of their orientation [20,21]. In general in these lattice models each spin represents a cluster of neighboring molecules whose short-range order is assumed to be maintained through the temperature range examined [36]. The one constant approximation case, i.e., $\lambda = \mu = \rho = 0$, reduces Eq. (2) to the well-known LL potential which correctly reproduces the orientational order across the nematic isotropic phase transitions [36]. The bulk nematic-isotropic (NI) transition for the LL model occurs at a reduced temperature [23] $T^* \equiv kT/\epsilon = 1.1232$. In the GHRL model, as is apparent in the equal elastic constants limit, we have a rescaling of the interaction strength, depending on the values of the elastic constants. This is taken care of by choosing the parameter Λ so that in all cases $\nu = -1$ (see Table I).

From a practical point of view, here we perform Metropolis Monte Carlo simulations [37] of the nematic films with homeotropic (along z) anchoring at the top and uniform alignment along x at the bottom, as illustrated in Fig. 1. When

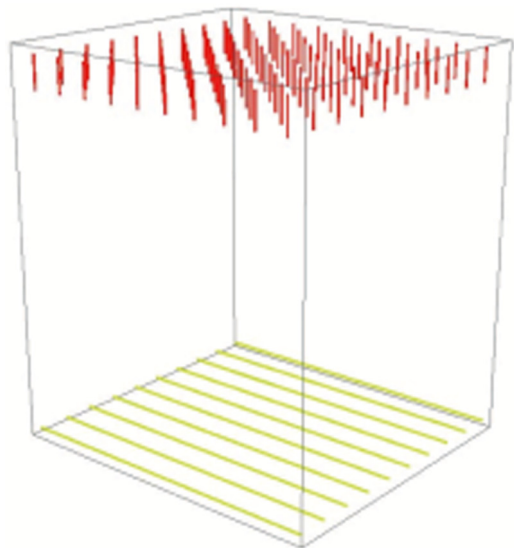


FIG. 1. A schematic representation of the homeotropic and homogeneous aligned boundary conditions at the top and bottom surfaces. We employ periodic boundary conditions at the other four faces of the lattice.

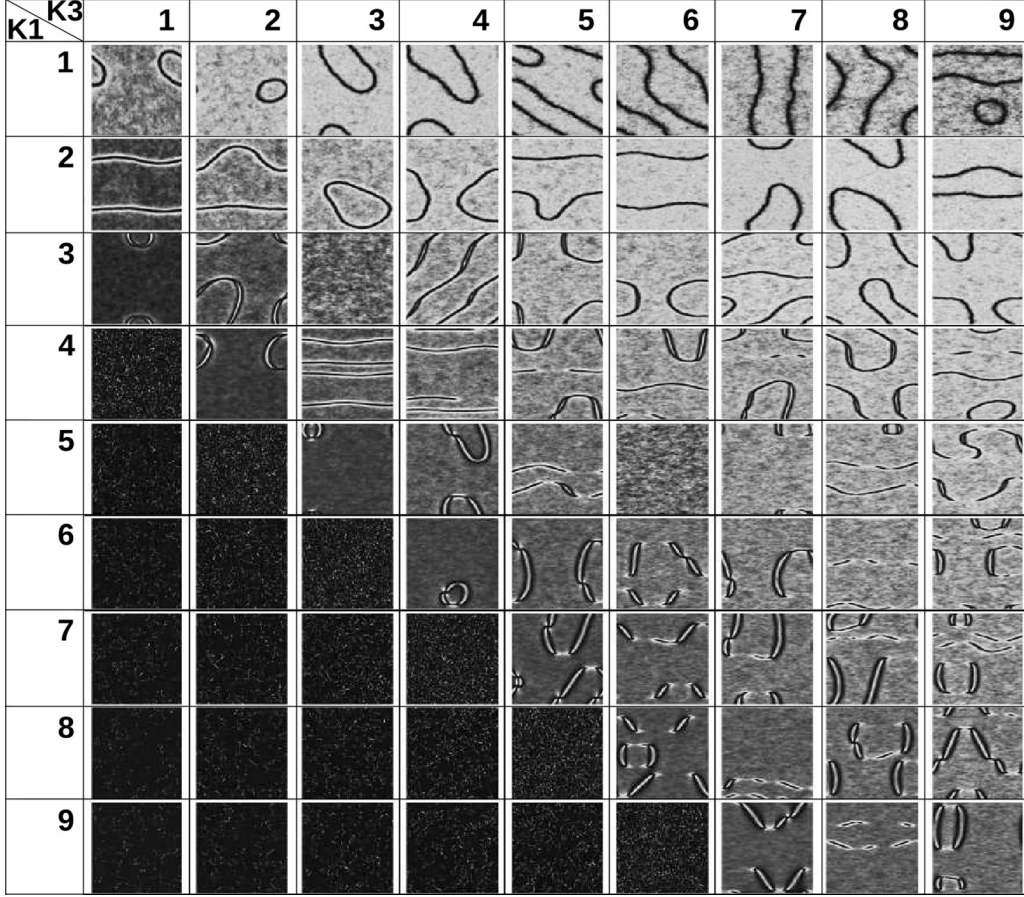


FIG. 2. Simulated optical patterns for a hybrid nematic film as obtained from a Monte Carlo simulation of a GHRL potential for different values of the three main elastic constants $K_i^* = K_i/10^{-12}$ N, $i = 1, 2, 3$. Here, the images are from $(K_1^* = 1, K_3^* = 1)$ (top left) to $(K_1^* = 1, K_3^* = 9)$ (top right) and from $(K_1^* = 9, K_3^* = 1)$ (bottom left) to $(K_1^* = 9, K_3^* = 9)$ (bottom right) while $K_2^* = 1$ is kept fixed.

dealing with confined systems, the boundary conditions are conveniently implemented, as we have done here, by additional layers of particles, with orientations kept fixed during the simulation, chosen to mimic the desired surface alignment [36], while at the other four faces of the sample we have used the periodic boundary conditions (PBCs) normally employed in simulating bulk systems [36]. We have already simulated these hybrid films in previous work, but either in the one-constant approximation [38,39] or with the aim of studying the effect of anchoring strength [16], while here we focus on the relation between elastic constant anisotropy and polarized optical images. In all the present simulations the starting configurations of the lattice were chosen to be completely aligned along the z direction and the evolution of the system was followed according to the classic Metropolis Monte Carlo procedure [40]. Each film was then considered to be placed between crossed linear polarizers and polarizing microscope (POM) textures were simulated by means of a Müller matrix approach [41,42], assuming the molecular domains, represented by the spins, to act as retarders on the light propagating through the sample [43]. The following parameters were employed for computing the optical textures: film thickness $d = 5.3 \mu\text{m}$, ordinary and extraordinary refractive indices $n_o = 1.5$ and $n_e = 1.66$, and light wavelength $\lambda_0 = 545 \text{ nm}$.

III. SIMULATIONS AND RESULTS

As mentioned before, here we have investigated the effect that changing the parameters depending on the elastic constants in the GHRL potential has on the POM textures. An example of the relation among the elastic constants, $K_i^* = K_i \times 10^{12}$ N, and the parameters λ , μ , ρ , and ν , appearing in the potential, is reported in Table I. We used a lattice with $200 \times 200 \times (10 + 2)$ spins and set the anchoring parameter to $J = 0.5$, then the spins interacted with the surface with half of the strength that they interacted with each other. Moreover, the reduced temperature was set to $T^* = 0.4$. The simulated optical images as obtained by considering crossed polarizers, placed at 45° and 135° , are presented in Figs. 2–4.

The simulations were first performed for the reference case of the single elastic constant approximation ($K_1 = K_2 = K_3$) using the LL model, and the results can be seen in the top left-hand panels of Figs. 2–4. Starting from these values we have then modified the relative strengths of K_1 , K_2 , and K_3 to examine the effects on the textures.

In Fig. 2, we show the results obtained keeping the twist constant fixed to $K_2 = 1$ and varying the splay and bend constants. We notice that for small K_1 , disclination lines and loops appear for all the values of K_3 examined. No defect is created when increasing the splay constant and making it greater than the bend one. When the splay and bend constants are of about

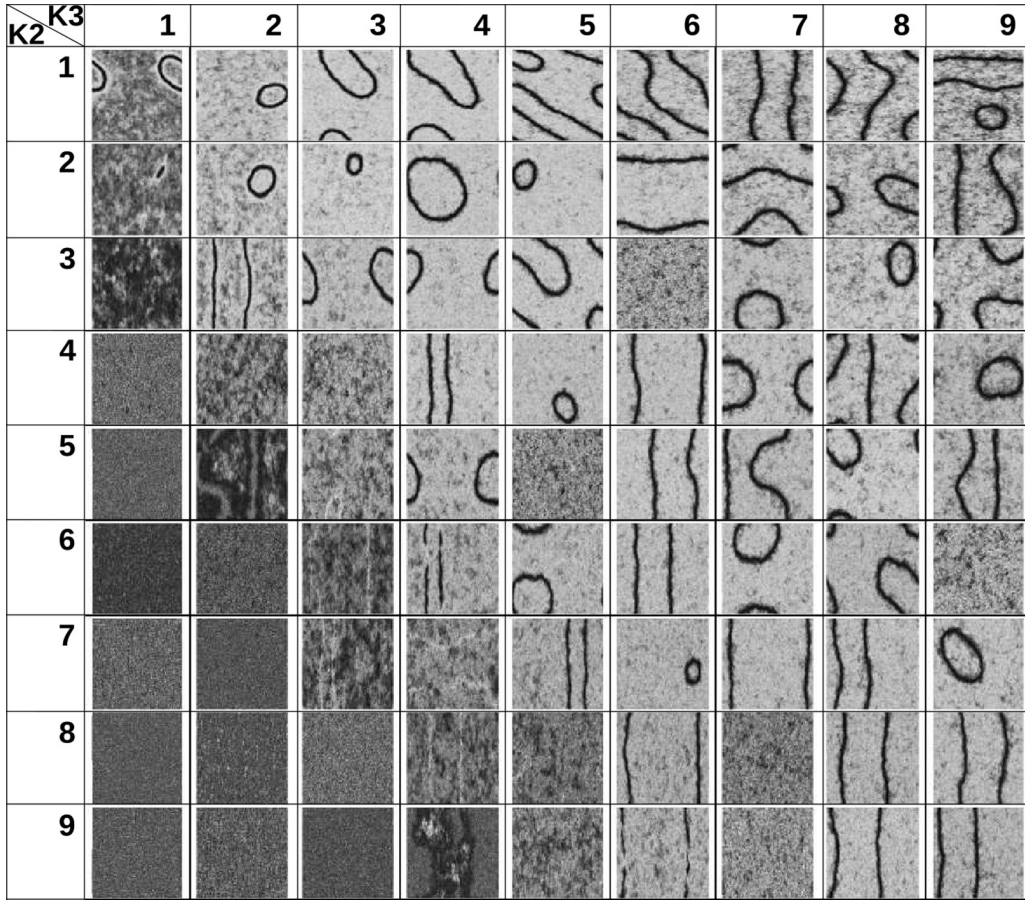


FIG. 3. Simulated optical patterns for a hybrid nematic film as obtained from a Monte Carlo simulation of a GHRL potential for different values of the three main elastic constants $K_i^* = K_i/10^{-12}$ N, $i = 1, 2, 3$. Here, the images are from $(K_2^* = 1, K_3^* = 1)$ (top left) to $(K_2^* = 1, K_3^* = 9)$ (top right) and from $(K_2^* = 9, K_3^* = 1)$ (bottom left) to $(K_2^* = 9, K_3^* = 9)$ (bottom right) while $K_1^* = 1$ is kept fixed.

the same values and much greater than the twist one, the appearance of four brush defects is clear. These defects evolve in two brushes increasing the value of K_3 .

Keeping the splay constant fixed to 1 and varying K_2 and K_3 , we can see that, apart from high values of the twist constant and high values of K_3 , in all the studied cases we have the formation of disclination lines if $K_3 \geq K_2$, as can be seen in Fig. 3. When the twist constant overcomes the bend one, again no defects appear, some light is transmitted, and then the corresponding images are gray.

Keeping $K_3 = 1$ fixed and varying K_2 and K_1 (see Fig. 4) we notice that for low values of the twist constant and high values of the splay one, we have an absence of defects because of the tendency of the molecules to orient themselves from the x direction of the bottom surface to the z direction of the top one in a uniform way. The light does not cross the film and consequently the textures are black.

Similarly to the case presented in Fig. 3, if the twist constant overcomes the bend one, again no defects appear, and the textures are gray and not black because some light is transmitted across the polarizers.

For similar values of K_2 and K_1 we have the appearance of inversion walls, i.e., two-dimensional regions where the director is not defined. Inversion walls are typically created following the relaxation of a homogeneous sample in a suitable geometry where the transient appearance of the defect

can be stabilized. There are various types of defect walls, e.g. splay-bend, bend-splay, and twist walls [1,2,7]. In particular, the liquid crystal can be subject to twist deformations, corresponding to rotations around a defined and unique axis, which can be identified in the sample. In a region where the twist is uniform, the director remains orthogonal to the rotation axis describing a helix around it. However, since the nematics are formed by nonpolar and nonchiral molecules there is no preferred sense for the helix twist, as both directions for rotating around the axis have the same probability. An inversion wall is thus generated at each boundary between domains with opposite twist.

After the Monte Carlo equilibration runs, the cells appear divided in two regions where the orientations of the molecules are uniform. The two blocks are separated by a stripe region where the intensity of the transmitted light varies between maxima and minima, as is evident by looking at the snapshots of the middle layer. In a previous work on inversion walls [44], we have shown that the width and the persistence of the domain walls depend on the film thickness, i.e., by increasing the thickness the stripe width increases, and that a larger thickness gives a behavior similar to that of a thinner film where the coupling or anchoring of the molecules at the surfaces is weaker. This feature can be observed in the snapshots and order parameter isosurfaces plotted together in Figs. 5–8. In these plots it is possible to note that the region between the

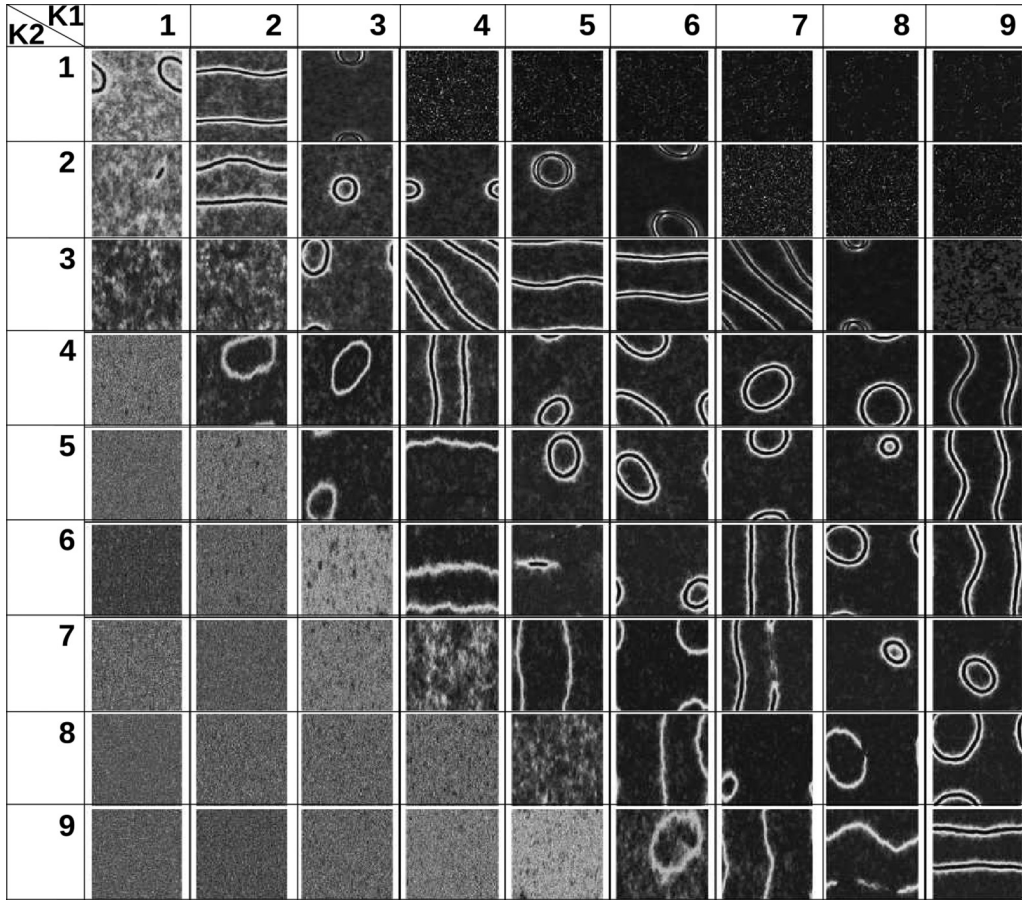


FIG. 4. Simulated optical patterns for a hybrid nematic film as obtained from a Monte Carlo simulation of a GHRL potential for different values of the three main elastic constants $K_i^* = K_i/10^{-12}$ N, $i = 1, 2, 3$. Here, the images are from $(K_2^* = 1, K_1^* = 1)$ (top left) to $(K_2^* = 1, K_1^* = 9)$ (top right) and from $(K_2^* = 9, K_1^* = 1)$ (bottom left) to $(K_2^* = 9, K_1^* = 9)$ (bottom right) while $K_3^* = 1$ is kept fixed.

defects is tilted in opposite directions. Moreover, we can see that the defects are placed closer to the bottom surface. In order to avoid such defects we are focusing on here, in a previous work [16] we implemented a tiny pretilt in the planar surface, which caused a break in these degenerate states, and thus a perfectly uniform sample could be analyzed.

In the majority of the cases in which defects are observed, the appearance of closed defect lines is remarkable. In some of them, they closely resemble elliptic curves. Indeed, this kind of behavior was predicted many years ago in uniform nematic samples subjected to external fields, where the direction offered by the surfaces (easy direction) and the direction imposed by the external field are competing [14,46,47]. This competitive orienting aspect was observed experimentally, especially in nematic lyotropic liquid crystals in the presence of magnetic fields [47]. Using the elastic theory, under appropriate conditions, it was demonstrated that the ratio of the axes of the elliptical loop defect formed in the nematic film can be proportional to $\sqrt{K_1/K_2}$, $\sqrt{K_3/K_2}$, or $\sqrt{K_3/K_1}$, depending on the anchoring imposed by the surfaces and on the direction of the external applied field [14].

In our simulations, a robust behavior such as the one observed in Figs. 2–4, i.e., well-defined elliptical curves, is not observed in all the samples. In addition, when they are present, we cannot observe a significant change in the aspect ratio just by changing the elastic constants in the calculations. However,

in the cases shown in Figs. 5–8, we do observe a tendency of increasing the aspect ratio of the closed curves with the increasing of K_3 . In these figures, periodically repeated images were positioned in order to improve the view. Moreover, the images were taken by considering the nematic film between crossed polarizers placed at 45° and 135° .

Thus, despite the fact we were not able to strictly verify the relation proposed in Ref. [14] between the ellipses' aspect ratio and the elastic constants, the elastic mechanism that favors the displaying of the elliptical lines in systems subjected to an external field is quite similar to the one observed here. In fact, once the Fréedericksz threshold field intensity is reached, the average molecular orientation can shift in one of at least two degenerated directions, due to $\vec{n} \equiv -\vec{n}$ symmetry [46,48]. Hence, the defect lines are placed in the region of separation of domains of different orientations. As argued before, the same behavior is observed in hybrid films such as the ones we are dealing with here, as can be confirmed by looking closely at the snapshots presented in Figs. 5–8. Indeed, in these figures it is possible to observe that the defect line is placed between two regions in which the spins turn in different directions.

The defects observed in Figs. 9 and 10 seem to be slightly different. Differently from the case illustrated in Fig. 9, in Fig. 10 it is possible to note some point defects. In the first case, the spins seem to present more noise when distorting from planar to homeotropic alignment. In the second case,

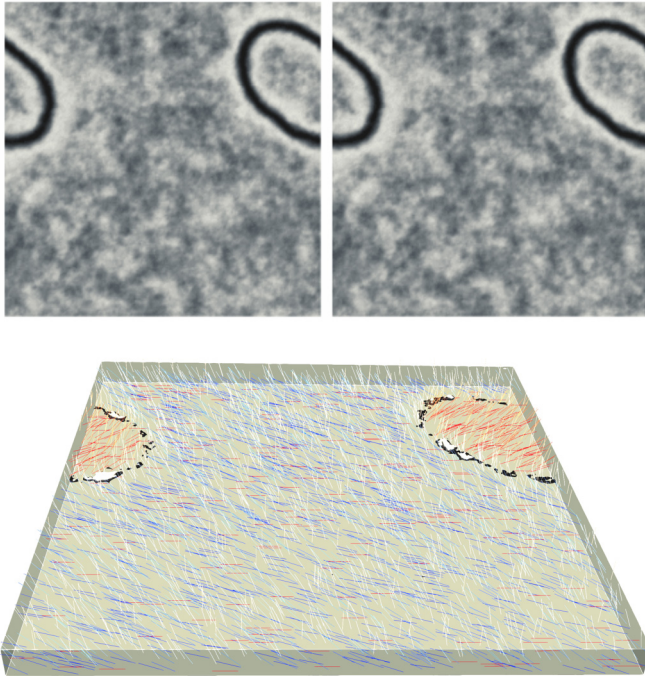


FIG. 5. Simulated optical pattern for a $200 \times 200 \times (10 + 2)$ nematic film for the elastic constants $K_1 = 1, K_2 = 1, K_3 = 1$. To better visualize the elliptic ring defect we have replicated the image obtained with the periodic boundary conditions. Bottom: Director field and order parameter isosurface obtained following the methodology presented in Ref. [45]. The white color encodes the director alignment along the z axis, while red and blue correspond to alignment along the positive and negative x axis, respectively. (Recall that the initial director orientation was along the positive z axis.) The order parameter isosurfaces were built by setting the c_l Westin metric [45] to 0.82.

however, the molecules seem to be more ordered, reaching a higher z component in a region close to the upper surface. Moreover, in Fig. 9, even in the defect core, close to the lower surface, the particles are not parallel to z , differently from what is shown in Fig. 10. By looking at the correspondent texture for the case presented in Fig. 9, in Fig. 2 (sixth line, fifth row), it is possible to notice that the textures are similar

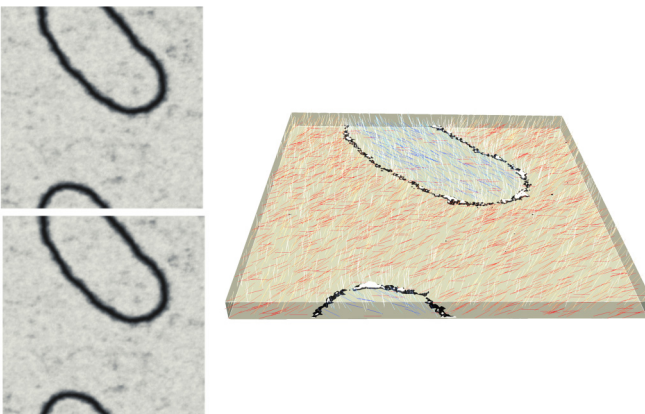


FIG. 6. As in Fig. 5 for $K_1 = 1, K_2 = 1, K_3 = 3$.

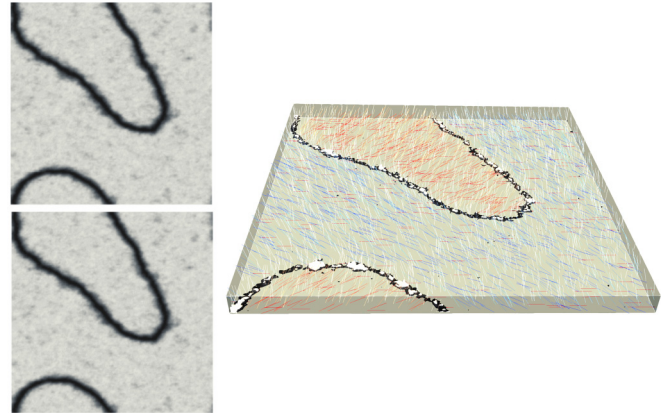


FIG. 7. As in Fig. 5 for $K_1 = 1, K_2 = 1, K_3 = 4$.

in the region of the map for which $K_1 \gg K_2$ and $K_3 \gg K_2$. In fact, since close to the lower surface it is more likely that the deformation is of splay type, while in the upper surface it is more likely to observe a deformation of a bend type, in this case, both kinds of distortions cost more energy. Then, the deformation from planar to homeotropic is smooth. Those textures are quite similar to the ones found in experiments with an applied external field and associated with Néel walls [49–51].

IV. CONCLUSIONS

We have performed a systematic Monte Carlo study to investigate the combined effects of elastic constant anisotropy

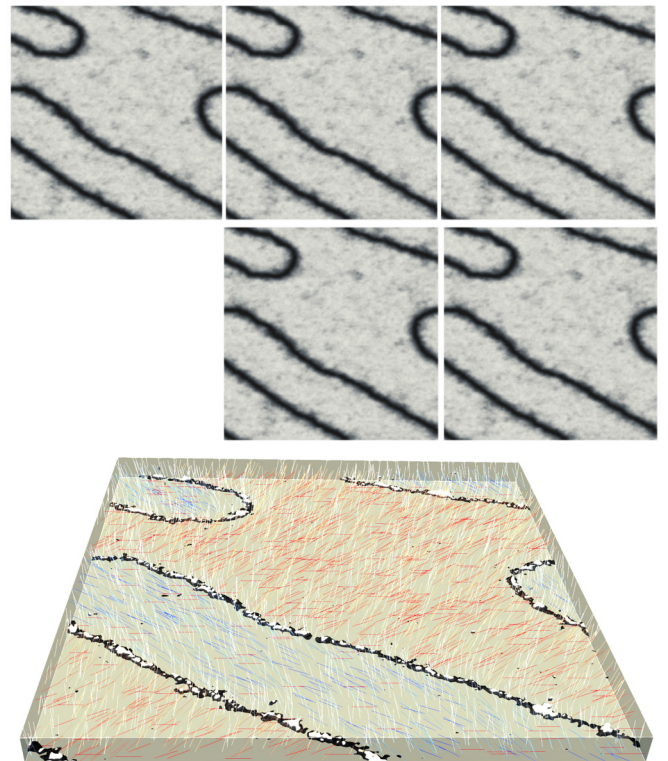


FIG. 8. As in Fig. 5 for $K_1 = 1, K_2 = 1, K_3 = 5$.

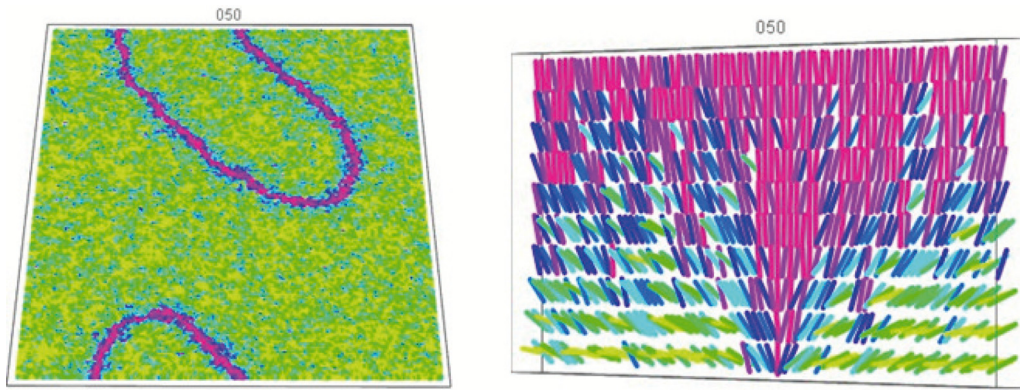


FIG. 9. Snapshots of a portion of the first bottom nematic layer (left) and a vertical cut of the system crossing the ring defect (right) for $K_1 = 1$, $K_2 = 1$, $K_3 = 3$.

and surface alignment on the textures of a hybrid nematic film. We have presented the simulated polarized optical images as obtained by varying the splay, twist, and bend elastic constants in order to produce an atlas of images corresponding to the numerous cases studied.

We have then produced a set of textures which can be useful to understand experimental data by comparing the simulated images with the real obtained ones when available or to predict the results of new experiments. In fact, knowing the elastic constant values of the nematic used, the simulated configurations could be of help in determining the kind of boundary conditions in real droplet systems in situations

where this is unknown. On the other hand, looking at the real POM images and knowing the surface orientation, it should be possible to give a rough estimate of the elastic constant anisotropies in a number of cases.

ACKNOWLEDGMENTS

L.R.E. and R.T.S. acknowledge financial support from CNPq, Capes, and Fundação Araucária (Brazil), and they also thank the INFN-Sezione Bologna (Italy) for partially supporting the visits to Bologna.

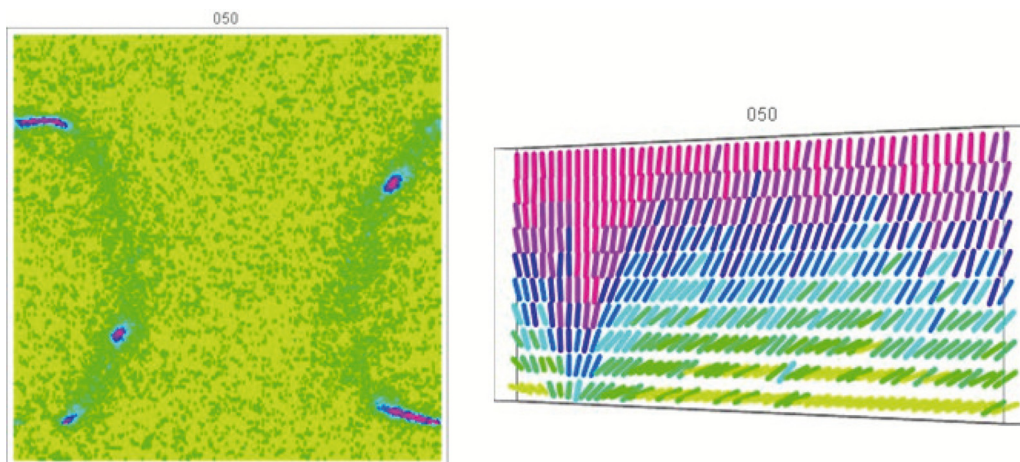


FIG. 10. Snapshots of a portion of the first bottom nematic layer (left) and a vertical cut of the system close to a point defect (right) for $K_1 = 6$, $K_2 = 1$, $K_3 = 5$.

-
- [1] P. G. de Gennes and J. Prost, *The Physics of Liquid Crystals* (Oxford University Press, Oxford, UK, 1993).
 - [2] S. Chandrasekhar, *Liquid Crystals*, 2nd ed. (Cambridge University Press, Cambridge, UK, 1992).
 - [3] S. Uchino, M. Kobayashi, and M. Ueda, Bogoliubov theory and Lee-Huang-Yang corrections in spin-1 and spin-2 Bose-Einstein condensates in the presence of the quadratic Zeeman effect, *Phys. Rev. A* **81**, 063632 (2010).
 - [4] S. Yasui, C. Chatterjee, and M. Nitta, Phase structure of neutron 3P_2 superfluids in strong magnetic fields in neutron stars, *Phys. Rev. C* **99**, 035213 (2019).
 - [5] M. J. Bowick, L. Chandar, E. A. Schiff, and A. M. Srivastava, The cosmological Kibble mechanism in the laboratory: String formation in liquid crystals, *Science* **263**, 943 (1994).
 - [6] L. Faddeev and A. J. Niemi, Stable knot-like structures in classical field theory, *Nature (London)* **387**, 58 (1997).

- [7] M. Kleman, *Points, Lines and Walls: in Liquid Crystals, Magnetic Systems and Various Ordered Media* (Wiley, New York, 1982).
- [8] D. A. Dunmur, Measurements of bulk elastic constants of nematics, in *Physical Properties of Liquid Crystals: Nematics*, edited by D. A. Dunmur, A. Fukuda, and G. R. Luckhurst, EMIS Datareview Series Vol. 25 (IEE, London, 2001), pp. 216–229.
- [9] C. Chiccoli, P. Pasini, C. Zannoni, G. Skačej, H. Yoshida, T. Hiroshima, K. Sunami, T. Ouchi, and M. Ozaki, From point to filament defects in hybrid nematic films, *Sci. Rep.* **9**, 17941 (2019).
- [10] M. Buscaglia, G. Lombardo, L. Cavalli, R. Barberi, and T. Bellini, Elastic anisotropy at a glance: The optical signature of disclination lines, *Soft Matter* **6**, 5434 (2010).
- [11] Y. Q. Lu, X. Liang, Y. H. Wu, F. Du, and S. T. Wu, Dual-frequency addressed hybrid-aligned nematic liquid crystal, *Appl. Phys. Lett.* **85**, 3354 (2004).
- [12] G. Barbero and L. R. Evangelista, *An Elementary Course on the Continuum Theory for Nematic Liquid Crystals* (World Scientific, Singapore, 2000).
- [13] D. R. Link, M. Nakata, Y. Takahashi, K. Ishikawa, and H. Takezoe, Patterns in Hybrid Nematic Liquid Crystal Films: Topography and Topology, *Phys. Rev. Lett.* **87**, 195507 (2001).
- [14] L. Leger, Static and dynamic behaviour of walls in nematics above a Fredericks transition, *Solid State Commun.* **11**, 1499 (1972).
- [15] C. Chiccoli, P. Pasini, L. R. Evangelista, R. Teixeira De Souza, and C. Zannoni, Lattice spin simulations of topological defects in nematic films with hybrid surface alignments, *Int. J. Mod. Phys. C* **22**, 505 (2011).
- [16] C. Chiccoli, L. R. Evangelista, E. K. Omori, P. Pasini, R. T. Teixeira-Souza, and C. Zannoni, Computer simulation of a nematic hybrid cell: The effects of elastic anisotropy, *Mol. Cryst. Liq. Cryst.* **649**, 86 (2017).
- [17] T. Gruhn and S. Hess, Monte Carlo simulation of the director field of a nematic liquid crystal with three elastic coefficients, *Z. Naturforsch. A* **51**, 1 (1996).
- [18] S. Romano, Elastic constants and pair potentials for nematogenic lattice models, *Int. J. Mod. Phys. B* **12**, 2305 (1998).
- [19] S. Romano, Computer simulation study of a two-dimensional nematogenic lattice model based on the Gruhn-Hess interaction potential, *Phys. Lett. A* **302**, 203 (2002).
- [20] G. R. Luckhurst and S. Romano, Computer simulation study of a nematogenic lattice model based on an elastic energy mapping of the pair potential, *Liq. Cryst.* **26**, 871 (1999).
- [21] P. J. Le Masurier, G. R. Luckhurst, and G. Saielli, Monte Carlo lattice simulations of the elastic behaviour of nematic liquid crystals, *Liq. Cryst.* **28**, 769 (2001).
- [22] P. A. Lebowitz and G. Lasher, Nematic liquid crystal order—a Monte Carlo calculation, *Phys. Rev. A* **6**, 426 (1972).
- [23] U. Fabbri and C. Zannoni, A Monte Carlo investigation of the Lebowitz-Lasher lattice model in the vicinity of its orientational phase transition, *Mol. Phys.* **58**, 763 (1986).
- [24] M. Kleman, in *Liquid Crystallinity in Polymers: Principles and Fundamental Properties*, edited by A. Ciferri (VCH, New York, 1991).
- [25] W. H. Song, H. J. Tu, G. Goldbeck-Wood, and A. H. Windle, Elastic constant anisotropy and disclination interaction in nematic polymers II. Effect of disclination interaction, *Liq. Cryst.* **30**, 775 (2003).
- [26] S. Fraden, A. J. Hurd, R. B. Meyer, M. Cahoon, and D. L. D. Caspar, Magnetic-field-induced alignment and instabilities in ordered colloids of tobacco mosaic virus, *J. Phys. Colloq.* **46**, C3-85 (1985).
- [27] W. H. Song, I. A. Kinloch, and A. H. Windle, Nematic liquid crystallinity of multiwall carbon nanotubes, *Science* **302**, 1363 (2003).
- [28] L. S. Li, J. Walda, L. Manna, and A. P. Alivisatos, Semiconductor nanorod liquid crystals, *Nano Lett.* **2**, 557 (2002).
- [29] J. Hobdell and A. H. Windle, Topological point defects in liquid crystalline polymers, *Liq. Cryst.* **19**, 401 (1995).
- [30] A. Sonnet, A. Kilian, and S. Hess, Alignment tensor versus director: Description of defects in nematic liquid crystals, *Phys. Rev. E* **52**, 718 (1995).
- [31] A. Kilian and S. Hess, Derivation and application of an algorithm for the numerical calculation of the local orientation of nematic liquid crystals, *Z. Naturforsch. A* **44**, 693 (1989).
- [32] S. D. Hudson and E. L. Thomas, Frank Elastic-Constant Anisotropy Measured from Transmission-Electron-Microscope Images of Disclinations, *Phys. Rev. Lett.* **62**, 1993 (1989).
- [33] S. D. Hudson, J. W. Fleming, E. Gholz, and E. L. Thomas, Disclination core structure in rigid and semiflexible main-chain polymer nematic liquid-crystals, *Macromolecules* **26**, 1270 (1993).
- [34] T. Ohzono, J. Fukuda, K. Suzuki, and T. Yamaguchi, $\pm 1/2$ wedge disclinations stabilized by a sinusoidal boundary in a thin hybrid nematic liquid-crystal film, *Phys. Rev. E* **86**, 030701 (2012).
- [35] C. Chiccoli, P. Pasini, and C. Zannoni, Can elastic constants and surface alignment be obtained from polarized microscopy images of nematic droplets? A Monte Carlo study, *J. Mol. Liq.* **267**, 158 (2017).
- [36] *Advances in the Computer Simulations of Liquid Crystals*, edited by P. Pasini and C. Zannoni (Kluwer, Dordrecht, 2000).
- [37] M. P. Allen and D. J. Tildesley, *Computer Simulation of Liquids*, 2nd ed. (Oxford University Press, Oxford, UK, 2017).
- [38] C. Chiccoli, O. D. Lavrentovich, P. Pasini, and C. Zannoni, Monte Carlo Simulations of Stable Point Defects in Hybrid Nematic Films, *Phys. Rev. Lett.* **79**, 4401 (1997).
- [39] C. Chiccoli, P. Pasini, A. Šarlah, C. Zannoni, and S. Žumer, Structures and transitions in thin hybrid nematic films: A Monte Carlo study, *Phys. Rev. E* **67**, 050703(R) (2003).
- [40] N. Metropolis, A. W. Rosenbluth, M. N. Rosenbluth, A. H. Teller, and E. Teller, Equation of state calculations by fast computing machines, *J. Chem. Phys.* **21**, 1087 (1953).
- [41] F. Xu, H. S. Kitzerow, and P. P. Crooker, Electric-field effects on nematic droplets with negative dielectric anisotropy, *Phys. Rev. A* **46**, 6535 (1992).
- [42] E. Berggren, C. Zannoni, C. Chiccoli, P. Pasini, and F. Semeria, Computer simulations of nematic droplets with bipolar boundary conditions, *Phys. Rev. E* **50**, 2929 (1994).
- [43] R. Ondris-Crawford, E. P. Boyko, B. G. Wagner, J. H. Erdmann, S. Žumer, and J. W. Doane, Microscope textures of nematic

- droplets in polymer dispersed liquid crystals, *J. Appl. Phys.* **69**, 6380 (1991).
- [44] C. Chiccoli, P. Pasini, I. Feruli, and C. Zannoni, Computer simulations of inversion walls in nematic films, *Mol. Cryst. Liq. Cryst.* **558**, 160 (2012).
- [45] A. C. Callan-Jones, R. A. Pelcovits, V. A. Slavin, S. Zhang, D. H. Laidlaw, and G. B. Lorient, Simulation and visualization of topological defects in nematic liquid crystals, *Phys. Rev. E* **74**, 061701 (2006).
- [46] F. Brochard, Mouvements de parois dans une lame mince nématique, *J. Phys. (Paris)* **33**, 607 (1972).
- [47] M. Simões, A. J. Palangana, L. R. Evangelista, W. S. Braga, and F. S. Alves, Bend and splay elastic constants at a reentrant isotropic–calamitic–nematic phase transition, *Phys. Rev. E* **72**, 031707 (2005).
- [48] W. Helfrich, Alignment-Inversion Walls in Nematic Liquid Crystals in the Presence of a Magnetic Field, *Phys. Rev. Lett.* **21**, 1518 (1968).
- [49] M. J. E. O'Rourke, D.-K. Ding, E. L. Thomas, and V. Percec, Morphologies and energies of Neel inversion wall defects in a liquid crystal polyether, *Macromolecules* **34**, 6658 (2001).
- [50] K. Okubo, M. Kimura, and T. Akahane, Measurement of genuine azimuthal anchoring energy in consideration of liquid crystal molecular adsorption on alignment film, *Jpn. J. Appl. Phys., Part 1* **42**, 6428 (2003).
- [51] N. Iwata, Y. Yoshioka, K. Yazawa, and M. Tokita, Azimuthal anchoring coefficients of nematic liquid crystals on polystyrene brushes formed at the air surface of block copolymer monolayers, *Liq. Cryst.* **47**, 1078 (2020).